Structure and Dynamics of Photogenerated Triplet Radical Ion Pairs in DNA Hairpin Conjugates with Anthraquinone End Caps

8 AUTHORS, INCLUDING:

Raanan Carmielli
Weizmann Institute of Science
44 PUBLICATIONS **866** CITATIONS

SEE PROFILE

Arun Kalliat Thazhathveetil
Northwestern University
21 PUBLICATIONS **370** CITATIONS

SEE PROFILE

Yasuhiro Kobori
Kobe University
48 PUBLICATIONS **836** CITATIONS

SEE PROFILE

Frederick D Lewis
Northwestern University
320 PUBLICATIONS **9,152** CITATIONS

SEE PROFILE

Structure and Dynamics of Photogenerated Triplet Radical Ion Pairs in DNA Hairpin Conjugates with Anthraquinone End Caps

Raanan Carmieli,[†] Amanda L. Smeigh,[†] Sarah M. Mickley Conron,[†] Arun K. Thazhathveetil,[†] Masaaki Fuki,[‡] Yasuhiro Kobori,*[‡,§] Frederick D. Lewis,*[†] and Michael R. Wasielewski*[†]

[†]Department of Chemistry and Argonne-Northwestern Solar Energy Research (ANSER) Center, Northwestern University, Evanston, Illinois 60208-3113, United States

[‡]Department of Chemistry, Faculty of Science, Shizuoka University, 836 Ohya Surugaku, Shizuoka 422-8529, Japan

[§]PRESTO, Japan Science and Technology Agency (JST), 4-1-8 Honcho Kawaguchi, Saitama 332-0012, Japan

Ⓢ *Supporting Information*

ABSTRACT: A series of DNA hairpins (**AqGn**) possessing a tethered anthraquinone (Aq) end-capping group were synthesized in which the distance between the Aq and a guanine-cytosine (G-C) base pair was systematically varied by changing the number ($n − 1$) of adenine-thymine (A-T) base pairs between them. The photophysics and photochemistry of these hairpins were investigated using nanosecond transient absorption and time-resolved electron paramagnetic resonance (TREPR) spectroscopy. Upon photoexcitation, $^1{*}Aq$ undergoes rapid intersystem crossing to yield $^3{*}Aq$, which is capable of oxidizing purine nucleobases resulting in the formation of $^3(Aq^{-\bullet}Gn^{+\bullet})$. All $^3(Aq^{-\bullet}Gn^{+\bullet})$ radical ion pairs exhibit asymmetric TREPR spectra with an electron spin polarization phase pattern of absorption and enhanced emission (A/E) due to their different triplet spin sublevel populations, which are derived from the corresponding non-Boltzmann spin sublevel populations of the $^3{*}Aq$ precursor. The TREPR spectra of the $^3(Aq^{-\bullet}Gn^{+\bullet})$ radical ion pairs depend strongly on their spin−spin dipolar interaction and weakly on their spin−spin exchange coupling. The anisotropy of $^3(Aq^{-\bullet}Gn^{+\bullet})$ makes it possible to determine that the π systems of $Aq^{-\bullet}$ and $G^{+\bullet}$ within the radical ion pair are parallel to one another. Charge recombination of the long-lived $^3(Aq^{-\bullet}Gn^{+\bullet})$ radical ion pair displays an unusual bimodal distance dependence that results from a change in the rate-determining step for charge recombination from radical pair intersystem crossing for $n < 4$ to coherent superexchange for $n > 4$.
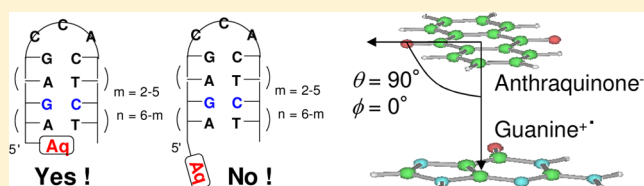
INTRODUCTION

Electron transport processes in DNA and the possibility of using DNA in nanoelectronic devices is the subject of extensive theoretical and experimental research.[1,2] The efficiency of photoinduced charge separation in DNA, like that in other electron donor-bridge-acceptor (D-B-A) systems, is limited by the competition between charge transport through the bridge molecules and charge recombination in the initially formed contact radical ion pair (CRIP). DNA conjugates in which the π-stacked base pairs of DNA provide multiple bridging units separating the donor and acceptor have proven particularly useful for understanding this competition (Scheme 1a, D-B$_n$-A).[3−6] Moreover, the ability to vary the number and sequence of base pairs as well as the donor and acceptor via solid-supported synthesis makes DNA well-suited for such studies. Charge separation over multiple base pairs occurs via a multistep mechanism consisting of photo-induced charge separation (k_{CS}) to form the initial CRIP or exciplex followed by charge transport across the bridge and charge trapping (k_{CT}) to form a charge-separated radical ion pair (Scheme 1a, SRIP).[7−9] The efficiency of SRIP formation is determined by the competition between charge transport and CRIP radiative and non-radiative decay to the ground state (k_{CT} vs k_{CCR}). Rate constants for non-radiative charge recombination of singlet CRIPs are energy gap dependent, in accord with Marcus theory for electron transfer.[10] Rate

Scheme 1. (a) Mechanism for Photoinduced Charge Separation in a Donor-Bridge-Acceptor (DBA) System Having an Excited Acceptor and Three Bridging Units; (b) Dynamics and Efficiency of Photoinduced Charge Separation for AqA and AqGn Systems[a]
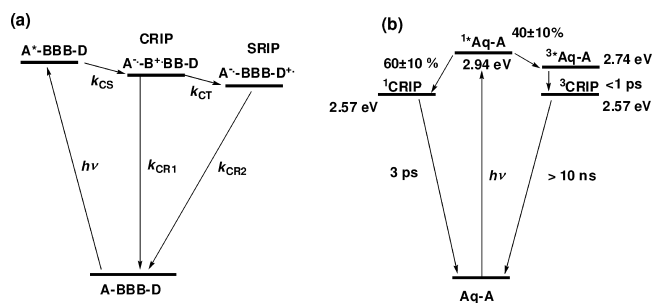
[a]Energies are from ref 21.

constants for hole transport across DNA bridges depend upon the number and sequence of the base pairs and are highest for

poly(purine) sequences (A-tracts or G-tracts).[7,11−13] Once formed, the singlet SRIP typically decays via a single-step superexchange mechanism, the rate constant for which is strongly distance dependent, also in accord with electron transfer theory.[14,15] Thus singlet D-B_n-A systems with short bridges have larger efficiencies for SRIP formation but shorter SRIP lifetimes than D-B_n-A systems with longer bridges.

One solution to the dual problems of low formation efficiencies and fast charge recombination for singlet SRIPs is the use of triplet excited states as electron acceptors. Anthraquinone (Aq) derivatives undergo rapid intersystem crossing and have been widely used in studies of photoinduced electron transfer in DNA.[16−20] However, the dynamics and efficiency of charge separation and charge recombination in Aq-DNA systems have received relatively little attention. Charge recombination of either a triplet CRIP or SRIP to form the singlet ground state is spin forbidden and thus potentially slower than charge transport over multiple base pairs in D-B_n-A systems with DNA base-pair bridges. We have reported the results of an investigation of the ultrafast dynamics and efficiency of singlet and triplet charge separation in the Aq-DNA conjugates **AqG1−AqG5**.[21] The efficiency of formation of long-lived triplet CRIPs (ca. 40% for **AqG2−AqG5** and ca. 25% for **AqG1**) is determined by the competition between singlet Aq charge transfer and Aq intersystem crossing (Scheme 1b). The triplet CRIPs do not decay on the time scale of our femtosecond experiments (0−6 ns).

In previous studies we have used a combination of transient optical absorption spectroscopy and time-resolved EPR spectroscopy (TREPR) to develop a more complete picture of charge transfer and spin dynamics in DNA hairpins.[22,23] In these studies we used perylene-3,4:9,10-bis(dicarboximide) (PDI) as the electron acceptor. PDI is a sufficiently powerful singlet photo-oxidant to quantitatively inject holes into adjacent adenine (A) and guanine (G) nucleobases. When PDI is used as a base pair surrogate within the duplex structure,[22] the charge-transfer dynamics observed following hole injection from PDI into the A-tract of the DNA hairpins is consistent with formation of a polaron involving an estimated 3−4 A bases. In a hairpin having 3 A-T base pairs between PDI and G, the SRIP that results from trapping of the hole by G is spin-correlated and displays TREPR spectra at 295 and 85 K that are consistent with its formation from ¹*PDI by the radical-pair intersystem crossing (RP-ISC) mechanism.[24−26] Charge recombination is spin-selective and produces ³*PDI, which at 85 K exhibits a spin-polarized TREPR spectrum that is diagnostic for its origin from the spin-correlated radical ion pair. Interestingly, in a hairpin having no G bases, TREPR spectra at 85 K reveal a spin-correlated radical pair with a dipolar interaction identical to that of having 3 A-T base pairs between PDI and G, implying that the A-base in the fourth A-T base pair away from the PDI chromophore serves as a hole trap. Thus, TREPR spectroscopy provides a level of structural detail that cannot be readily obtained using transient optical spectroscopy.

As we pointed out earlier,[21] obtaining structural information on transient intermediates is especially important in the case of the Aq-capped hairpins because of the flexible linker joining Aq to the end of a single DNA strand. Thus we have used a combination of nanosecond transient optical and TREPR spectroscopy to determine both the charge recombination dynamics and the structure of the SRIP formed following selective photoexcitation of Aq within Aq-DNA conjugates **AqG1−AqG7**, which contain a single G hole trap, and **AqA**, which lacks a hole trap. The triplet SRIP spectra recorded by TREPR were analyzed using the theory developed by Kobori et al.[27] for photoinduced ET via the excited

triplet state. This theory is used to describe transfer of the non-Boltzmann populations of the ³*Aq spin sublevels to those of the ³($Aq^{-\bullet}Gn^{+\bullet}$) radical ion pair that is formed with rate constant k'_{CS} (Scheme 2). This not only allows us to calculate the spin−spin

Scheme 2. Triplet Spin Sublevels within ³*Aq and ³($Aq^{-\bullet}Gn^{+\bullet}$) and the Possible Population Transfer Pathways
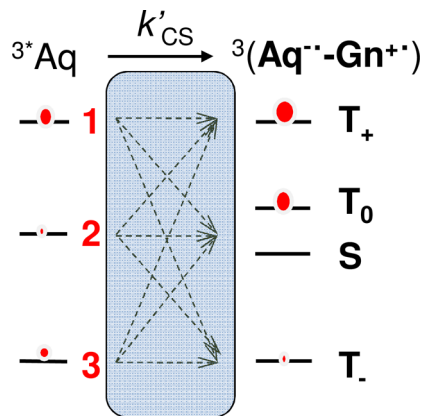
exchange and dipolar interactions in ³($Aq^{-\bullet}Gn^{+\bullet}$), but also provides the distance and orientation of $G^{+\bullet}$ and $Aq^{-\bullet}$ relative to one another in the charge separated state. The charge recombination kinetics are compared to those for hairpins having the singlet acceptor stilbenedicarboxamide (Sa) hairpin linker separated from G by 0−5 A-T base pairs (**SaG1−SaG6**, Chart 1).[28]

Chart 1. Structure of Anthraquinone and Stilbene Capped Hairpins and Anthraquinone (Aq) and Stilbenedicarboxamide (Sa)
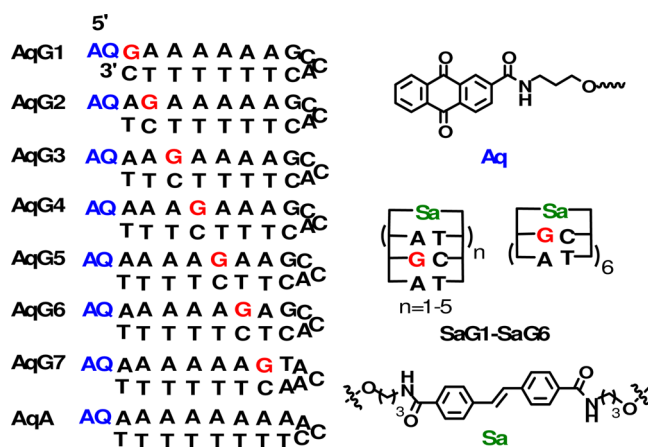
EXPERIMENTAL SECTION

Synthesis and Characterization. The synthesis and characterization of conjugates **AqG1−AqG5** have been previously described.[21] Preparation of **AqG6**, **AqG7**, and **AqA** employed similar methods. Their MALDI-TOF mass spectra and melting temperatures are reported in Supplementary Table S1. Briefly, *N*-(3-hydroxypropyl) anthraquinone-2-carboxamide was synthesized by the procedure of Gasper and Schuster[29] and incorporated into the oligonucleotide conjugates shown in Chart 1. The conjugates were characterized by MALDI-TOF mass spectrometry, UV and circular dichroism (CD) spectroscopy, and melting temperatures (Supplementary Table S1 and Figure S1). They form hairpin structures in which the Aq is assumed to serve as a capping group[29] attached to the polypurine strand, and the midstrand GACCC or CCA sequences form mini-hairpin loops.[11,30] The hairpin stem

regions possess either all A-T base pairs (**AqA**) or a single G-C base pair located at a variable distance from Aq (**AqG***n*, *n* =1−7). The UV spectra of the conjugates display a weak long-wavelength band at 340 nm assigned to the Aq n−π^* transition and a stronger band at 260 nm dominated by nucleobase absorption (Supplementary Figure S1A). The CD spectra are characteristic of B-DNA structures possessing multiple A-T base pairs (Supplementary Figure S1B).[11] The thermal dissociation profiles in 10 mM sodium phosphate buffer (pH 7.2) with 100 mM NaCl (the standard buffer employed in all of the spectroscopic studies) provide melting temperatures of 60 ± 1 °C at 295 K, which decrease to 35 ± 1 °C when the buffer is diluted 1:1 with ethylene glycol for experiments at 85 K (Supplementary Figure S1C).

Nanosecond Transient Absorption Spectroscopy. Nanosecond transient absorption spectra for **AqG1**–**AqG7** were obtained at 295 K and for **AqG2** and **AqG4** at 85 K as described in the Supporting Information by exciting deoxygenated samples having similar 355 nm absorbances with 7 ns, 2 mJ, 355 nm laser pulses generated using the frequency-tripled output of a Continuum 8000 Nd:YAG laser.[8,31]

TREPR Spectroscopy. DNA samples for EPR measurements were prepared in the following way: 0.8 mM DNA sample in 10 mM sodium phosphate buffer (pH 7.2) with 100 mM NaCl and 20% glycerol was loaded into quartz tubes (3.8 mm o.d., 2.4 mm i.d.) and subjected to several freeze−pump−thaw degassing cycles on a vacuum line (10−4 Torr). The tubes were then sealed with a hydrogen torch. TREPR measurements using continuous wave (CW) microwaves and direct detection were carried out using a Bruker Elexsys E580 X-Band EPR spectrometer outfitted with a variable Q dielectric resonator (ER-4118X-MD5-W1). The temperature was controlled by an Oxford Instruments CF935 continuous flow cryostat with an optical window using liquid N₂. Samples were photoexcited at 355 nm (0.5 mJ/pulse, 7 ns, 10 Hz) using the frequency-tripled output from a Nd:YAG laser (QuantaRay Lab 150). The polarization of the laser was set to 54.7° relative to the direction of the static magnetic field to avoid magnetophotoselection effects on the spectra. Following photoexcitation, kinetic traces of transient magnetization were accumulated under CW microwave irradiation (typically 6−20 mW). The field modulation was disabled to achieve a time response of $Q/\pi\nu \approx 30$ ns, where Q is the quality factor of the resonator and ν is the resonant frequency, while microwave signals in absorption (*a*) and/or emission (*e*) were detected in both the real and the imaginary channels (quadrature detection). Sweeping the magnetic field gave 2D spectra versus both time and magnetic field. For each kinetic trace, the signal acquired prior to the laser pulse was subtracted from the data. Kinetic traces recorded at magnetic field values off-resonance were considered background signals, whose average was subtracted from all kinetic traces. A PDI-DNA sample prepared in a 0.8 mm o.d. thin-walled quartz tube was used as an internal standard for phase alignment of the EPR spectra and recorded using 532 nm photoexcitation.[22] Simulation of the powder-pattern spectra of the triplet-born SRIP signals[27] were performed using a home-written MATLAB[32] program.

■ RESULTS

Transient Optical Absorption Spectroscopy. Transient absorption spectra of **AqG5** obtained between 360 and 600 nm with 10 nm increments following a 7 ns, 355 nm laser pulse are shown in Figure 1. The spectra display maxima near 400 and 525 nm with band shapes similar to those previously reported for Aq$^{-\bullet}$.[33] The decays of the 525 nm transient absorbance for **AqG1**–**AqG7** and **AqA** display only minor variations in initial absorbance (Supplementary Figure S2). Normalized decays are shown in Figure 2. First order fits to the average of two or more transient decays for **AqG1**–**AqG5** provide the decay times reported in Table 1. Similar decay times were obtained for the 400 nm transients. The 525 nm transients for **AqG6** and **AqG7** decay only slightly during the 4.5 μs duration of these experiments, whereas that of **AqA** is incomplete within 4.5 μs. The 525 nm transient decays for **AqG6** and **AqA** obtained on the 0−1.8 ms time scale are shown in Figure 3. Their decays are largely complete on this time scale and provide the decay times reported in Table 1.
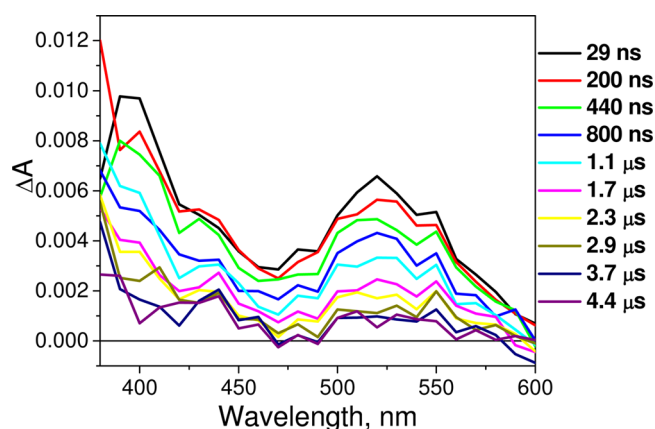

Figure 1. Transient absorption spectra of **AqG5** following excitation with a 7 ns, 355 nm laser pulse in 10 mM phosphate buffer (pH 7.2, 100 mM NaCl). The spectra were obtained over the range 360−600 at 10 nm increments with decay times from 29 ns to 4.4 μs.
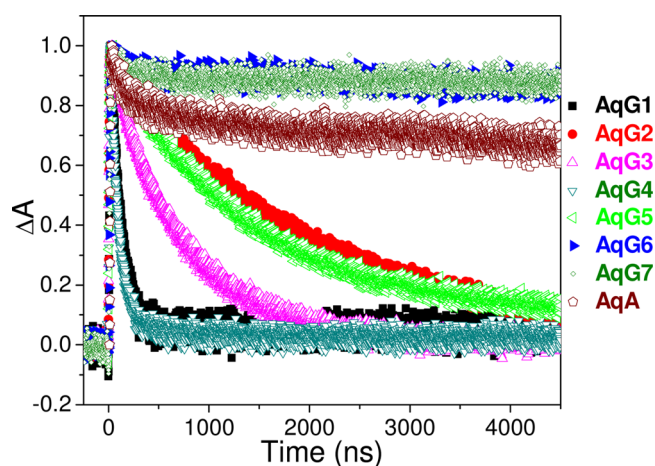

Figure 2. Normalized transient decays at 525 nm following excitation with a 7 ns, 355 nm laser pulse for conjugates **AqG1**−**AqG7** and **AqA** in 10 mM phosphate buffer (pH 7.2, 100 mM NaCl).

Table 1. Decay Times of Aq$^{-\bullet}$ and Rates of Recombination at 525 nm for Aq Capped DNA Hairpins after 355 nm Excitation in 10 mM Phosphate Buffer, pH 7.2 (100 mM NaCl)

hairpin	τ_{CR2} (μs)	k_{CR2} (s^{-1})
AqG1	0.110 ± 0.006	9.1 ± 0.5 × 10⁶
AqG2	2.1 ± 0.1 (4 ± 1)[a]	4.9 ± 0.3 × 10⁵
AqG3	0.65 ± 0.12 (0.46 ± 0.05)[b]	1.6 ± 0.3 × 10⁶
AqG4	0.099 ± 0.015 (7.2 ± 0.5)[a]	1.0 ± 0.2 × 10⁷
AqG5	1.37 ± 0.09	7.3 ± 0.5 × 10⁵
AqG6	196 ± 20	5.1 ± 0.5 × 10³
AqG7	670 ± 190	1.5 ± 0.4 × 10³
AqA	290 ± 4	3.5 ± 0.1 × 10³

[a]In 1:1 ethylene glycol/10 mM phosphate buffer pH 7.2 (10 mM NaCl) at 85 K. [b]Without nitrogen purging.

The 525 nm transient decay for **AqG7** remains incomplete on this time scale. UV spectra recorded prior to and following laser excitation displayed little or no change in band shape and intensity.

The effect of deoxygenation by purging with nitrogen was investigated in the case of **AqG3**. The decay time for an **AqG3** solution in air is 0.46 μs, somewhat shorter than the value for the deoxygenated sample (Table 1). Transient decays were also determined for **AqG2**
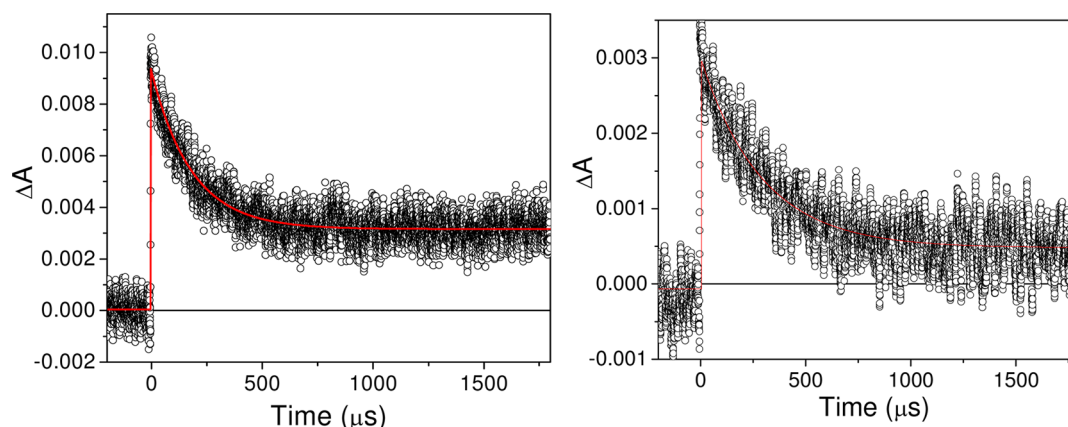
Figure 3. Transient decay at 525 nm following excitation with a 7 ns, 355 nm laser pulse for **AqG6** (left) and **AqA** (right) in 10 mM phosphate buffer (pH 7.2, 100 mM NaCl).

and **AqG4** in 50% ethylene glycol/buffer without deoxygenation at 295 K and at 85 K (Supplementary Figure S3). The decrease in the maximum ΔA observed in the kinetic traces at 85 K relative to those measured at 295 K indicates that the quantum yield of charge separation is about three times lower at 85 K. Decay times obtained from single exponential fits are reported in Table 1 and Supplementary Table S1. The decay times are longer at 85 K than at 295 K.

TREPR Spectroscopy. Following photoexcitation of **AqG2–AqG5** with a 355 nm, 7 ns laser pulse, TREPR spectra with an A/E electron spin polarization pattern were observed at 85 K (Figure 4),
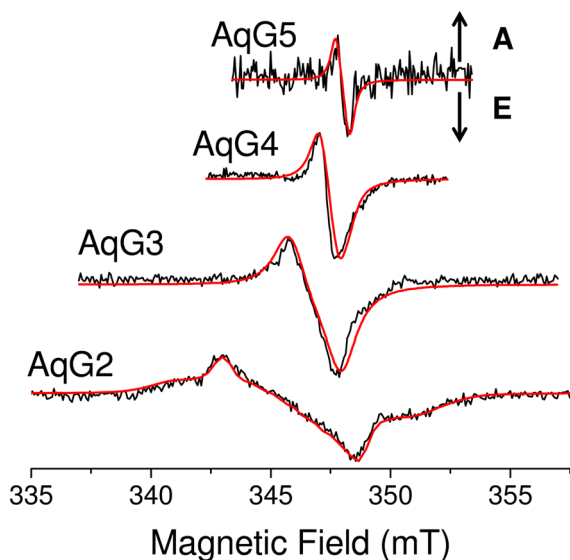

Figure 4. TREPR spectra of **AqG2–AqG5** at 85 K following excitation with a 7 ns, 355 nm laser pulse. The smooth curves superimposed on the experimental spectra are computer simulations of the radical pair spectra with the parameters given in Table 2.

where A and E denote enhanced absorption and emission, respectively. Figure 4 shows that the spectral width depends on the position of G relative to Aq in the hairpin, resulting from changes in the spin–spin dipolar (d) and exchange (J) interactions between the unpaired electrons of the SRIP, which are distance dependent. The TREPR spectra were simulated using the triplet–triplet electron spin polarization transfer (ESPT) model developed by Kobori et al.,[27] which will be described in more detail below. **AqG5** exhibits a weaker TREPR signal compared to those of **AqG2–AqG4**, and no signal was observed for **AqG6** and **AqG7**. This most likely results from the

charge separation quantum yield of **AqG5–AqG7** being very low at 85 K. The simulation parameters are summarized in Table 2.

Table 2. Simulation Parameters for SRIP Spectra for AqG2–AqG5 Measured by TREPR at 100 ns after a 7 ns, 335 nm Laser Pulse

hairpin	d (mT)	J (mT)	k'_{CS} (s^{-1})	r (Å)
AqG2	−6.0	0−1.0	1.2×10^{11}	7.7
AqG3	−1.8	0−0.2	1×10^{11}	11.6
AqG4	−0.9	0−0.2	9×10^{10}	14.6
AqG5	−0.4	0−0.2	9×10^{10}	19.1

The spectral simulations were used to determine both the distance and orientation of G$^{+\bullet}$ relative to Aq$^{-\bullet}$. The zero-field splitting parameters of ^{3}*Aq used in the simulations are $D = -351$ mT and $E = 5$ mT.[34] The initial value for the dipolar interaction (d) between the spins in Aq$^{-\bullet}$ and G$n^{+\bullet}$ was calculated assuming that the base pair stacking distance is 3.4 Å, and d was subsequently varied to fit the experimental spectra. In addition, the position and the orientation of G$^{+\bullet}$ with respect to Aq$^{-\bullet}$ were first determined in **Aq$^{-\bullet}$G2$^{+\bullet}$** by using (1) θ and ϕ values for the position of G$^{+\bullet}$ and (2) Euler angles α, β, and γ for the molecular orientation (Supplementary Figure S4) because the spectrum for this SRIP is better resolved than the others. The remaining spectra were then simulated using the set of angles obtained for **Aq$^{-\bullet}$G2$^{+\bullet}$** as a starting point. Figure 5 shows the spectral simulations for **Aq$^{-\bullet}$G2$^{+\bullet}$** and their dependence on molecular geometry (Figure 6 and Supplementary Table S5), where it can be seen that $\theta = 90°$, $\phi = 0°$, $\alpha = 90°$, $\beta = 90°$, and $\gamma = 0°$ yields the best fit. This data shows that Aq$^{-\bullet}$ is π-stacked parallel to the bases of the DNA hairpin since G2$^{+\bullet}$ is constrained by its neighboring bases to a parallel π-stacked geometry.

Figure 7 shows the AqG2 spectral simulations as a function of J with a fixed parallel Aq$^{-\bullet}$ orientation relative to G2$^{+\bullet}$. It can be seen that the simulated spectra depend weakly on J with the largest deviations from the experimental spectra occurring when J is small and negative. In contrast, when $|J| > 1$ mT, the spectral simulations again are insensitive to the magnitude of J.

Figure 8 shows how the simulated TREPR spectral lineshape of ^{3}(**Aq$^{-\bullet}$G2$^{+\bullet}$**) depends on the photoinduced charge separation rate constant. Since the Kobori model treats the charge separation as a single-step event, the rate constant obtained from the simulation should be viewed as an overall effective rate constant for the process (k'_{CS}). The spectral simulations of ^{3}(**Aq$^{-\bullet}$G$n^{+\bullet}$**), where $n = 2-5$, all yield similar charge separation rate constants (Table 2).
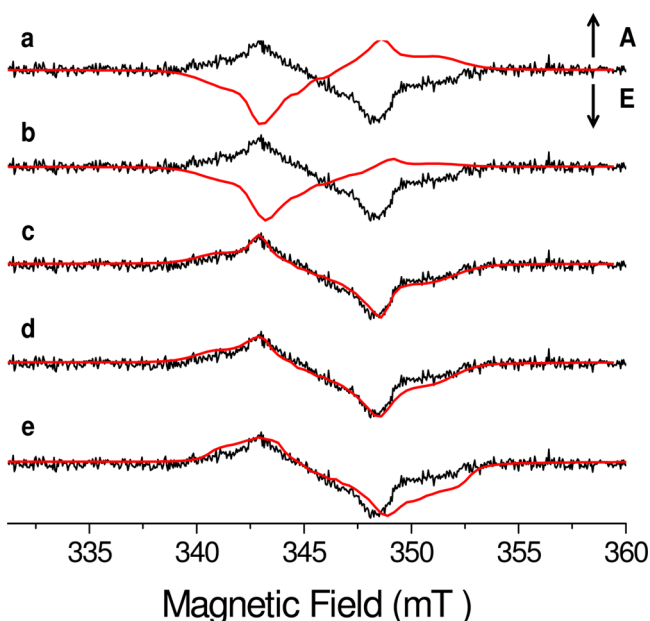
Figure 5. Simulation (red trace) of **Aq2G** TREPR spectrum (black trace) at 85 K following excitation with a 7 ns, 355 nm laser pulse as a function of θ, ϕ, α, β and γ. The corresponding geometries used for the calculations are shown in Figure 6.

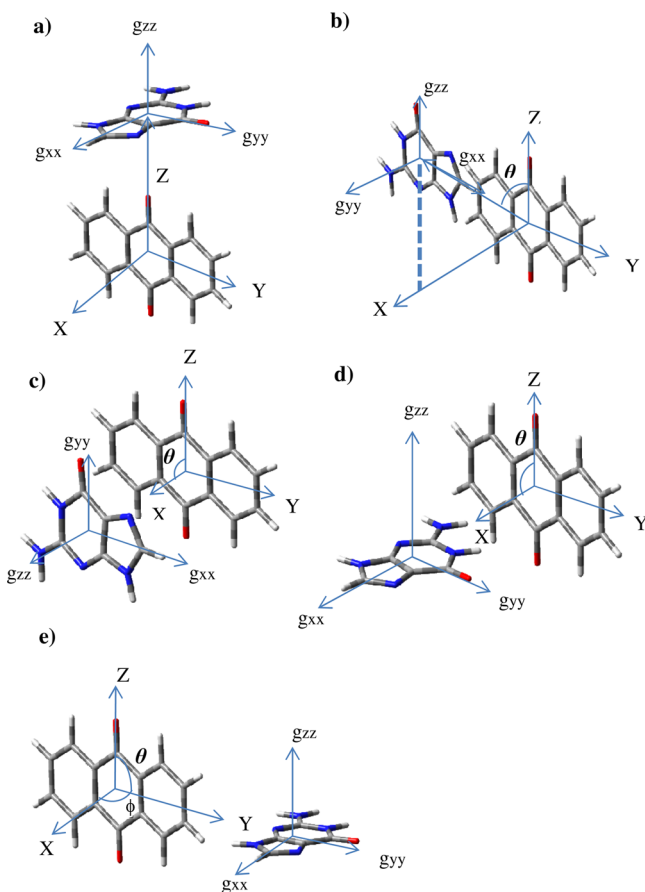**Figure 6.** Molecular geometries of the SRIP considered for the spectral simulations in Figure 5.

Interestingly, the kinetic traces of the $^3(\mathrm{Aq}^{-\bullet}\mathrm{G}n^{+\bullet})$ TREPR spectra, where $n = 2-5$, all exhibit the same 300 ns monoexponential decay (data not shown). Since the charge recombination time constants

for $^3(\mathrm{Aq}^{-\bullet}\mathrm{G}n^{+\bullet})$ obtained from the nanosecond transient absorption measurements at 85 K for **AqG2** and **AqG4** are 4 and 7 μs, respectively, we attribute the 300 ns decay of the TREPR signal to spin relaxation rather than charge recombination (Scheme 1a, k_{CR2}).

■ DISCUSSION

Transient Optical Spectroscopy. We previously proposed that the conjugates **AqG1−AqG5** adopt capped hairpin structures similar to those for stilbene-capped hairpins[35,36] in which the ACC sequence forms a mini-hairpin loop and the Aq attached to the poly(purine) strand is π-stacked with the terminal base pair.[21] The solution structure of a self-complementary duplex having π-stacked Aq groups at either end has recently been reported.[37] All of the Aq conjugates have melting temperatures >58 °C (in the absence of ethylene glycol) and are assumed to be fully base-paired at room temperature. Their UV spectra display a weak long-wavelength band at 340 nm assigned to the Aq n,π* transition and a stronger band at 260 nm dominated by nucleobase absorption. Their CD spectra are characteristic of B-DNA structures possessing multiple A-T base pairs.[38]

Our previous investigation of the femtosecond time-resolved transient absorption spectra of **AqG1−AqG5** established that the 400 and 525 nm transient absorption bands characteristic of the anion radical Aq$^{-\bullet}$ are formed within 1 ps following laser excitation.[21] The mechanism for formation and decay of Aq$^{-\bullet}$ with a neighboring A summarized in Scheme 1b is consistent with earlier proposals by Schuster and co-workers.[39,40] Competition between singlet electron transfer and ^{1*}Aq → ^{3*}Aq intersystem crossing followed by triplet electron transfer results in the formation of both singlet and triplet CRIPs. The former decays rapidly ($\tau \approx 3$ ps) via charge recombination, whereas the latter does not decay within the maximum pump−probe delay of our femtosecond transient absorption apparatus (0−6 ns). The quantum yield for formation of the long-lived triplet CRIP is determined by the competition between Aq singlet electron transfer and intersystem crossing. Faster singlet electron transfer for neighboring G versus A results in a lower efficiency for neighboring G ($\Phi_{\mathrm{cs}} \approx 0.25$ vs 0.40 for A). Faster singlet electron transfer may also account for the lower efficiencies for formation of long-lived SRIP's in hairpin conjugates having Aq attached to the poly(pyrimidine) versus poly(purine) strand[21] and in the duplex systems studied by Kawai et al.[20]

The 400 and 525 nm transient absorption bands of **AqG1−AqG6** assigned to Aq$^{-\bullet}$ undergo decay on the nanosecond to millisecond time scale (Figures 1−3). The decays of these bands display first-order kinetics, as expected for an intramolecular charge recombination mechanism (Scheme 1a). The 525 nm **Aq$^{-\bullet}$G$n^{+\bullet}$** decay times for **AqG1−AqG6** are reported in Table 1, and the rate constants for charge recombination of the charge-separated radical ion pair ($k_{\mathrm{CR2}} = \tau^{-1}$) are plotted in Figure 9 versus n, the location of the guanine hole trap, along with our data for the Sa-linked hairpins **SaG1−SaG6** (Chart 1).[28,41] The distances shown at the top of the figure are estimated assuming a normal average B-DNA base stacking distance of 3.4 Å. The decay time for **AqG3** is faster in the presence of air than in deoxygenated solutions (Table 1), consistent with collisional electron transfer from long-lived Aq$^{-\bullet}$ to O$_2$.

Salient features of our data include (a) similar initial yields of Aq$^{-\bullet}$ from **AqG1−AqG7** and **AqA**, (b) decay times that increase with increasing distance for **AqG2−AqG4** and decrease with distance for **AqG4−AqG6**, and (c) multiexponential decay for **AqA**. The first of these features was noted at short delay times in our earlier femtosecond investigation of charge separation in **AqG1−AqG5**[21] and at longer decay times by Kawai and co-workers in their investigation of Aq-capped duplexes.[20]
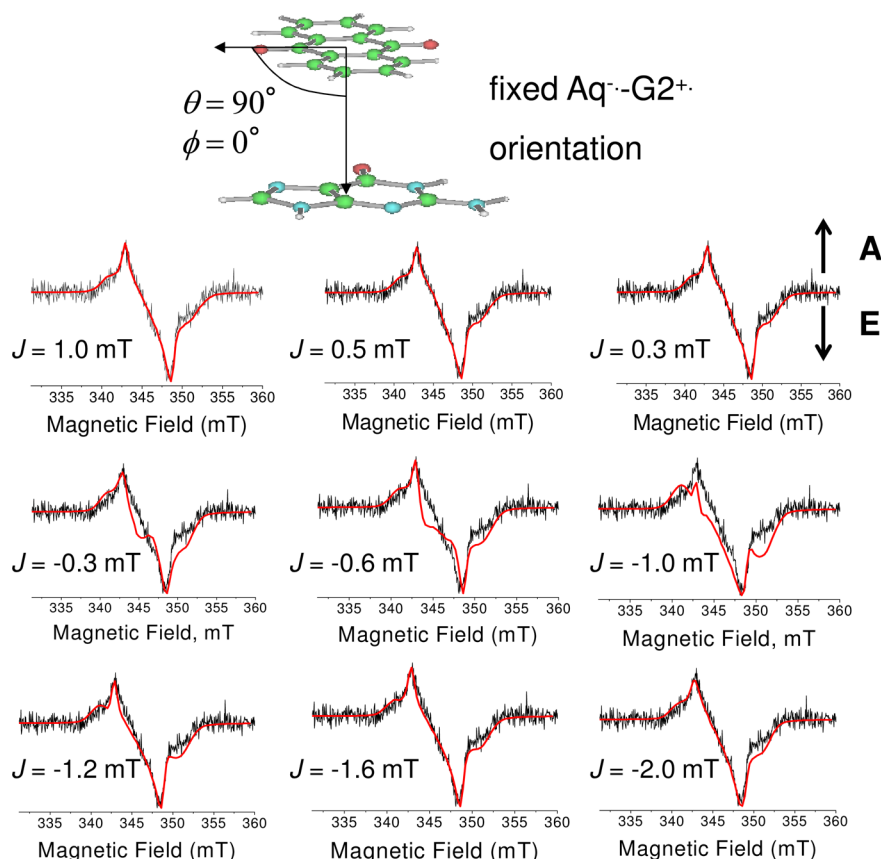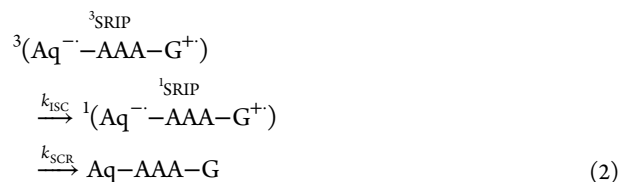
Figure 7. Experimental **AqG2** spectra (black traces) at 85 K ns following excitation with a 7 ns, 355 nm laser pulse and their simulations (red traces) as a function of J.

The similar initial intensities for the transient absorption decays for **AqG1**−**AqG7** at 295 K (Supplementary Figure S2) are indicative of similar quantum yields for formation of the long-lived SRIPs, independent of D−A distance. This result indicates that A-tract hole transport and hole trapping by G (Scheme 1a, k_{CT}) is much faster than ^{3}CRIP charge recombination (k_{CCR}) for all of the Aq conjugates. Hole arrival times at G have not been determined for the **AqGn** systems because the transient absorption of G$^{+\bullet}$ is too weak be detected in our transient absorption measurements.[42] However, hole arrival times are expected to be similar to those we have reported for stilbene donor-bridge-acceptor systems with A-tract bridges.[12] For example, the hole arrival time on G for **SaG7**, which is analogous to **AqG7**, is 8.3 ns and thus substantially faster than even the **Aq$^{−\bullet}$G1$^{+\bullet}$** decay time (Table 1). Thus there is ample time for the initially formed CRIP to undergo hole transport across the A-tract followed by hole trapping by G prior to CRIP charge recombination.

The values of k_{CR2} for the stilbene-linked hairpins **SaG1**−**SaG6**[28] provide a benchmark against which our Aq data can be evaluated. Both the Sa and Aq systems possess a photo-oxidant (Sa or Aq) separated from a guanine electron donor by an A-tract of variable length (Chart 1). The plot of log(k_{CR2}) versus n for **SaG1**−**SaG6** is linear when $n > 1$, as expected for a bridge-mediated coherent superexchange electron transfer process.[43,44] The value of log(k_{CR2}) for **SaG1** lies close to this line but is excluded from the linear fit because there is no bridging unit separating the donor and acceptor in this hairpin. The slope of the plot of log(k_{CR2}) vs R, the D−A distance according to eq 1 provides a value of $\beta = 0.94$ Å^{-1} for the bridge attenuation factor.

$$k_{CR2} = k_0 \, e^{-\beta(R - R_0)} \qquad (1)$$

Values of k_{CR2} for **AqG1**-**AqG3** are substantially slower than those for the corresponding Sa-linked hairpins (Figure 9), e.g., the ratio of rate constants for **SaG2/AqG2** is 14,000/1! These enormous rate ratios are attributed the spin-forbidden nature of charge recombination for the triplet SRIPs formed by **AqG2** and **AqG3** as well as the triplet CRIP formed by **AqG1**. Charge recombination of the triplet radical ion pairs to produce the ground state requires that triplet-singlet RP-ISC, k_{ISC}, occurs prior to electron transfer from the singlet radical ion pair to ground state, k_{SCR}:

$$^3(\text{Aq}^{-\bullet}-\text{AAA}-\text{G}^{+\bullet}) \overset{^3\text{SRIP}}{}$$
$$\xrightarrow{k_{ISC}} {}^1(\text{Aq}^{-\bullet}-\text{AAA}-\text{G}^{+\bullet}) \overset{^1\text{SRIP}}{}$$
$$\xrightarrow{k_{SCR}} \text{Aq}-\text{AAA}-\text{G} \qquad (2)$$

Assuming that the rate constants for singlet superexchange in the **AqGn** and **SaGn** systems are similar, the slower charge recombination rate constants k_{CR2} observed for **AqG1**−**AqG3** vs **SaG1**−**SaG3** indicate that triplet-singlet intersystem crossing is the rate-determining step for Aq$^{−\bullet}$ decay in these systems ($k_{ISC} \ll k_{SCR}$). The observed values of k_{CR2} for **AqG2**−**AqG4** increase with distance (Figure 9). It is well-known that k_{ISC} increases with distance as the singlet−triplet splitting between the $^1(\text{Aq}^{−\bullet}\text{G}n^{+\bullet})$ and $^3(\text{Aq}^{−\bullet}\text{G}n^{+\bullet})$ radical ion pairs decreases as reflected by a decrease in J and d.[45] Neglecting the nuclear hyperfine interactions in each radical, the RP-ISC rate constant for T$_0 \rightarrow$ S, k_{ISC}, can be estimated as[46−49]

$$k_{ISC} \cong \frac{k_{SCR}(\Delta g \beta B_0 \hbar^{-1}/2)^2}{(J + (d/2))^2 + (\Delta g \beta B_0 \hbar^{-1}/2)^2} \qquad (3)$$
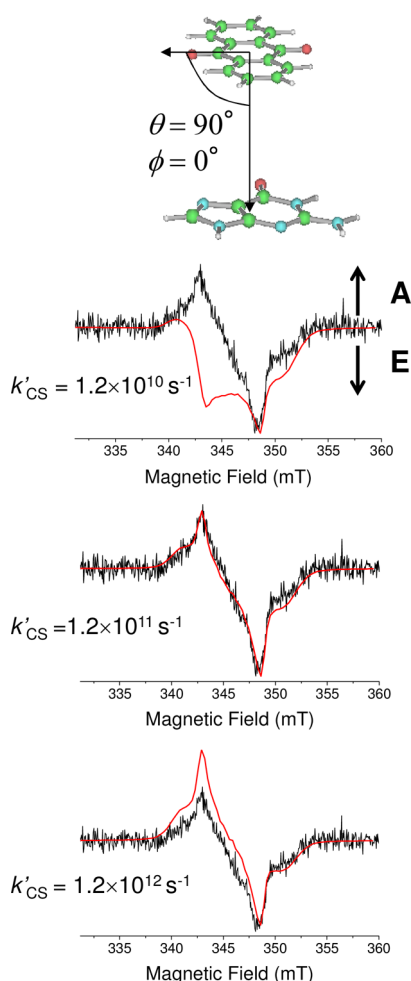
Figure 8. Simulations (red traces) of the **AqG2** TREPR spectrum (black trace) at 85 K ns following excitation with a 7 ns, 355 nm laser pulse as a function of the reaction rate, k'_{CS}.
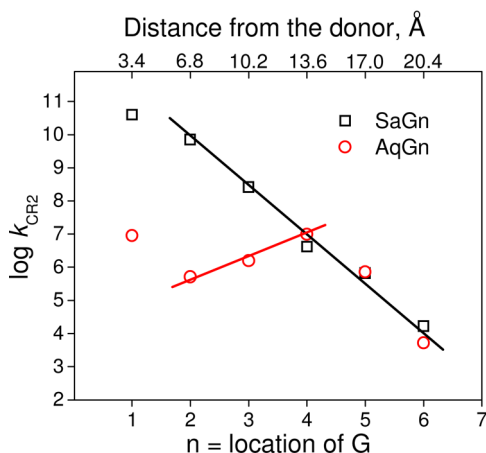

Figure 9. Dependence of the first-order rate constant for charge recombination of the charge-separated radical ion pairs (SRIP) from **AqGn** and **SaGn** conjugates on the location of G (bottom X-axis) or the distance between the acceptor and G (upper X-axis).

where Δg is the g-factor difference between the two radicals, β is the Bohr magneton, and B_0 is the applied magnetic field. This expression is based on the idea that rapid charge recombination to the singlet ground state provides an important singlet–triplet dephasing pathway for

spin-correlated radical pairs. For example, since the charge recombination rate within $\mathbf{Aq^{-\bullet}Gn^{+\bullet}}$ is dominated entirely by k_{SCR} when $n = 5-7$ (Figure 9), $k_{CR2} \cong k_{SCR}$, so that extrapolating the log k_{CR2} versus distance data for **AqG5–AqG7** back to the Aq-G distance in **Aq–G2** gives $k_{SCR} = 7 \times 10^9$ s^{-1}. Using this value as well as J and d measured for **AqG2** (Table 2) in eq 3 yields $k_{ISC} \cong 10^6$ s^{-1}, which is consistent with the observed value of k_{CR2} for **AqG2**. In a related observation, a modest decrease in triplet SRIP lifetimes has been observed for alkane-linked porphyrin-viologen compounds with increasing chain length (4–8 methylenes); however, interpretation of these results is complicated by conformational heterogeneity of the linker.[50]

Values of k_{CR2} for **AqG4–AqG6** are similar to those for **SaG4–SaG6**. Since k_{ISC} increases with increasing D–A distance,[45] it is not surprising that electron transfer rather than RP-ISC is the rate-determining step for charge recombination in systems with large D–A distances (eq 2, $k_{CR2} > k_{ISC}$). It is interesting to note that the values of k_{CR2} for **AqG4–AqG6** are similar to those for **SaG4–SaG6** even though the energy gap between the radical ion pair and ground state is smaller for the Aq systems as a consequence of the much more positive Aq reduction potential (-0.88 V[33] compared to -1.91 V[41] for Sa vs SCE in acetonitrile). Electron transfer theory shows that k_{CR2} depends on the electronic coupling matrix element (V_{CR2}) for this process as well as its reaction free energy (ΔG_{CR2}) and total nuclear reorganization energy $\lambda = \lambda_I + \lambda_S$, where λ_I is the internal reorganization energy of the donor and acceptor and λ_S is the solvent reorganization energy:[51−53]

$$k_{CR2} = \frac{2\pi}{\hbar} |V_{CR2}|^2 \sqrt{\frac{1}{4\pi\lambda k_B T}} \, e^{-\left[\frac{(\Delta G_{CR2}+\lambda)^2}{4\lambda k_B T}\right]} \qquad (4)$$

The values of V_{CR2} for the series **AqG4–AqG6** and **SaG4–SaG6** should be similar because they depend largely on coupling between $G^{+\bullet}$ and the bridging A-tract states as is typical for the coherent superexchange mechanism.[43,44] Thus, on the basis of eq 4, the similar k_{CR2} values observed for the **AqG4–AqG6** and **SaG4–SaG6** series indicate that $[(\Delta G_{CR2} + \lambda)^2/\lambda]_{Sa} \cong [(\Delta G_{CR2})^2/\lambda]_{Aq}$ for these systems. Using $\Delta G_{CR2} \cong -3.0$ eV and $\lambda = 1.3$ eV reported for **SaG4**,[3] as well as $\Delta G_{CR2} = -2.12$ eV for the **AqG4–AqG6** systems obtained from the sum of the oxidation potential of G ($E^{ox} = 1.24$ V[3]) and reduction potential of Aq ($E^{red} = -0.88$ V), $\lambda \cong 0.8$ eV for the **AqG4–AqG6** systems. The internal reorganization energy for the **SaG4–SaG6** systems ($\lambda_I = 1.0$ eV)[3] is very large, so that the 0.5 eV decrease in λ in the **AqG4–AqG6** systems most likely results from a decrease in λ_I when Sa is replaced by the more rigid Aq. Sa has torsional degrees of freedom about the single bonds linking the phenyl groups to its central double bond, which contribute to the larger λ_I relative to that of Aq.

We have considered the possibility that slow charge recombination for the **AqGn** systems having longer A-tract bridges occurs via thermal repopulation of the bridge followed by hole transport and charge recombination of the singlet CRIP. Thermal repopulation of the bridge should be more favorable for the relatively shallow hole trap G than for the deeper hole traps such as the stilbenediether used in our studies of donor–acceptor capped hairpins[15] and the phenothiazine used by Majima and co-workers of charge recombination dynamics in donor–acceptor capped hairpins having A-tract bridges.[14] Yet the charge recombination rate constants for systems with 4–7 bridging adenines are similar for systems having G, stilbenediether, and phenothiazine hole traps. These observations are consistent with the slow rate constant for G-to-G hole transfer in a GAAAG sequence ($k_{CT} = 1.4 \times 10^4$ s^{-1}),[54] which provides an upper bound for the rate constant for thermal repopulation of the A$_n$ bridge from a G hole trap.

Further evidence for a tunneling versus hopping mechanism for charge recombination is provided by the temperature dependence of the Aq$^{-•}$ decay times for **AqG2** and **AqG4** in 50% ethylene glycol/buffer (Supplementary Table S1). The much lower initial intensity for **AqG4** at 85 K versus room temperature (Supplementary Figure S3 vs S2) is a likely consequence of the hopping mechanism for charge separation. We have recently shown that G-tract hole hopping is thermally activated.[8] The Aq$^{-•}$ decay times are significantly longer at 85 K versus room temperature for **AqG2** (4.0 vs 0.6 μs) and **AqG4** (7.3 vs 0.14 μs). Thus it is unlikely that either repopulation of the bridge or A-to-A hole transport, both of which are activated processes, occur at 85 K in the glassy medium.

The relatively high quantum yields for formation of the **AqA** CRIP (ca. 0.40) and spin-forbidden nature of charge recombination make it possible to observe the decay of Aq$^{-•}$ from **AqA** on the nanosecond–millisecond time scale (Figures 2 and 3). The distribution of decay times is suggestive of charge recombination from a distribution of SRIPs having different D–A distances. The slow component of the Aq$^{-•}$ decay (ca. 290 μs) accounts for approximately half of the total decay amplitude. This decay time is much longer than expected for charge recombination following an unbiased random walk in an A-tract with an A-to-A hopping rate of ca. 1×10^9 s^{-1}.[9] Slow charge recombination might be a consequence of local trapping within the A-tract, a phenomenon that we previously observed in conjugates possessing a PDI acceptor as a base-pair surrogate.[22] In addition, the A base in the ACC hairpin loop of **AqA** may provide a hole trap site.

TREPR Spectroscopy. TREPR measurements were used to determine the molecular conformation of the **Aq$^{-•}$G$n^{+•}$** SRIP state produced by electron transfer from ^{3*}Aq. Rapid spin–orbit-induced intersystem crossing (SO-ISC) in ^{1*}Aq to produce ^{3*}Aq is intrinsically anisotropic because the zero-field splitting of the triplet state resulting from the spin–spin dipolar interaction is anisotropic with respect to the principal molecular axes (X, Y, and Z) of the π system.[55] The anisotropic SO-ISC process produces non-Boltzmann populations of the three canonical zero-field X, Y, and Z spin sublevels, i.e., electron spin polarization (ESP), which can be transferred to the spin states of the CRIP and subsequently to those of the SRIP during the charge separation reaction when spin–lattice relaxation of the polarized triplet state is slower than the reaction rate (Scheme 2).[56,57] This is known as the triplet mechanism (TM) of chemically induced dynamic electron polarization (CIDEP). The intrinsic anisotropy of these processes make TREPR spectroscopy a powerful tool for determining the molecular geometry and the electronic properties of the **Aq$^{-•}$G$n^{+•}$** SRIP state. In addition, when the spin–spin exchange interaction, J, between the two radicals that constitute the radical pair is sufficiently small, the spin-correlated radical pair mechanism (SC-RPM), which involves RP-ISC, ^{3}(**Aq$^{-•}$G$n^{+•}$**) $\leftrightarrow$ ^{1}(**Aq$^{-•}$G$n^{+•}$**), can also lead to non-Boltzmann spin sublevel populations within the radical pair state.[24−26]

When the radical pair precursor state is a photoexcited triplet state, both mechanisms can be active and lead to a complex dependence of the overall radical pair spin polarization on the magnetic interactions within the radical pair. This complexity depends to large degree on the anisotropic properties of the triplet precursor and the subsequent triplet radical pair, so that a complete analysis of the system can yield structural information about the transient radical pair. Recently, Kobori et al. reported a theory and computational model describing radical pair formation from a spin-polarized photoexcited triplet state precursor,[27] which will be described here briefly. Upon photoexcitation, fast SO-ISC occurs from ^{1*}Aq to ^{3*}Aq with different population rates to each of the X, Y, and Z spin sublevels of ^{3*}Aq.[55] The

eigenvalues of the SRIP state are generally different from those of the photoexcited triplet precursor and are labeled X', Y' and Z'. If the SRIP spin–spin exchange interaction (J) is weak, the singlet SRIP spin state also participates in the description of the spin-correlated radical pair.

Two limiting cases are reported for triplet–triplet electron-spin polarization transfer (ESPT). The first one is the case of *fast charge transfer*, where k'_{CS} is much larger than the angular frequency of the Zeeman term, $g\beta B_0$. In this case, the off-diagonal elements in the density matrix that describes the spin system, i.e., the quantum coherences created when SO-ISC occurs, are not averaged to zero, so that these terms contribute to determining the overall sublevel populations in the radical pair state.[27] This is essentially equivalent to transferring the non-Boltzmann populations of the three canonical zero-field X, Y, and Z spin sublevels of ^{3*}Aq to the spin states of the CRIP and subsequently to those of the SRIP, provided that the values of k_{CS} and k_{CT} are much faster than spin relaxation. This results in the spectral asymmetry that is notably evident in the TREPR spectra of **AqG2**–**AqG5** (Figure 4). The second case involves *slow charge transfer*, where k_{CS} and/or k_{CT} are much smaller than the angular frequency of the Zeeman term, $g\beta B_0$. Once triplet spin polarization is generated in ^{3*}Aq, the slow follow-up charge separation reaction allows sufficient time for the off-diagonal elements in the density matrix describing the spin system to average to zero, i.e., the quantum coherences are lost, so that when the initial absorptive or emissive spin polarization in ^{3*}Aq is transferred to the CRIP state and then on to the SRIP state through ESPT, the TM results in so-called "net spin polarization". In the work presented here, a general case is considered where k_{CS} and/or k_{CT} can be comparable to the angular frequency of the Zeeman term. In this study, the oscillatory off-diagonal terms are revealed to be partially averaged to result in the very weak TM effect, contributing to the slightly asymmetric TREPR spectra as shown in Figure 4. (See Supporting Information for the computational method.)

The positions (ω_{ij}) of the four EPR transitions for the spin-correlated radical pair are[24−26,58]

$$\omega_{12} = \omega_0 - \Omega - J + d_{zz}$$
$$\omega_{34} = \omega_0 - \Omega + J - d_{zz}$$
$$\omega_{13} = \omega_0 + \Omega - J + d_{zz}$$
$$\omega_{24} = \omega_0 + \Omega + J - d_{zz} \tag{5}$$

where ω_0 is the center of the spectrum and

$$\Omega^2 = (J + d_{zz}/2)^2 + Q^2 \tag{6}$$

and

$$d_{zz} = d[3\cos^2(\xi) - 1] \tag{7}$$

where ξ is the angle between the dipolar axis of the radical pair and the direction of the magnetic field B_0. The mixing term Q between singlet and triplet states is

$$Q = \frac{1}{2}(g_1 - g_2)\beta B_0/\hbar + \frac{1}{2}\left(\sum a_{1i}m_{1i} - \sum a_{2j}m_{2j}\right) \tag{8}$$

where g_1 and g_2 are the g factors of radicals 1 and 2, and a_{1i} and a_{2j} are the hyperfine coupling constants of radicals 1 and 2 having m_{1i} and m_{2j} nuclei. Unlike the case of a spin-correlated radical pair originating from a singlet state, where the absolute intensities of the transitions are equal to the population of the S–T$_0$ sublevels, in the case of a spin-correlated radical pair originating from a triplet state, the intensities depend on the initial population of the triplet

sublevels and as a result the intensities of the transitions are not necessarily equal, so that the EPR spectrum can be asymmetric.

$$I_{12} = [\rho_{22}(t) - \rho_{11}(t)]\sin^2 \mu$$

$$I_{13} = [\rho_{33}(t) - \rho_{11}(t)]\cos^2 \mu$$

$$I_{24} = [\rho_{44}(t) - \rho_{22}(t)]\sin^2 \mu$$

$$I_{34} = [\rho_{44}(t) - \rho_{33}(t)]\cos^2 \mu \tag{9}$$

where $\sin \mu = [(\Omega - 2J - 2d)/2\Omega]^{1/2}$ and $\cos \mu = 2\Delta\omega/[2\Omega (\Omega - 2J - 2d)]^{1/2}$.

The magnitude of J depends exponentially on the distance r between the two radicals and is assumed to be isotropic, while that of d depends on $1/r^3$ and is anisotropic. For molecules in the solid state, d is not rotationally averaged to zero, and the value of d is usually approximated by the point dipole model:[59]

$$d = -\frac{3\mu_0 g^2 \beta^2}{8\pi r^3} \tag{10}$$

where μ_0 is the vacuum permeability. In units of mT and Å, $d = -2785$ mT·Å^3/r^3.

Analysis of the EPR spectra using the triplet−triplet ESPT model[27,60] allows us for the first time to determine the geometry of the capped Aq chromophore with respect to the first base-pair, because the polarization pattern is highly sensitive to the polar angles, θ and ϕ, and the Euler angles α, β, and γ defining the position and the orientation of G$^{+\bullet}$ relative to Aq$^{-\bullet}$. The calculated EPR spectrum is sensitive not only to the molecular position but also to the orientation of G$^{+\bullet}$,[60] since G$^{+\bullet}$ possesses highly anisotropic nitrogen hyperfine couplings (Table S4 and Figure S4).[61] From the spectral simulations with different angles, it was determined that Aq$^{-\bullet}$, although covalently attached to only one side of the DNA hairpin strand, is π-stacked to the first base-pair. This is also in agreement with the recently reported solution structure of a self-complementary duplex having π-stacked Aq groups at either end.[37]

Unfortunately, the spin−spin exchange interaction, J, could not be determined accurately from the simulations. Nevertheless, on the basis of the quality of the simulated data, the sign of J is most likely positive, but this requires further verification using a spin label acting as an observer spin. Polarization transfer from the SRIP to a third observer spin can be used to determine the sign of J.[62] However, according to the charge-transfer interaction model that predicts J for radical ion pairs,[63] the positive sign of the coupling is reasonable because the SRIP state is energetically located in the inverted region for the charge-recombination to the ground state, contributing to destabilization of the singlet SRIP by the electronic coupling perturbation. Since RP-ISC is the rate limiting step of charge recombination for **AqG1**−**AqG3**, J needs to be much larger than the Q value for S−T$_0$ mixing (eq 7).

The charge separation rates, k'_{CS}, obtained from simulating the spectra are all about 10^{11} s^{-1} with no apparent distance dependence (Figure 8). From the simulation, the derived k'_{CS} is comparable to the angular frequency of the Zeeman interaction for the experiments described here, where $g_e\beta_e B_0 \cong 10^{10}$ s^{-1}, so that the data can be interpreted as an intermediate case as explained earlier. Previous investigations of the femtosecond time-resolved transient absorption spectra of **AqG1**−**AqG5** obtained at room temperature established that the 400 and 525 nm transient absorption bands characteristic of the anion radical Aq$^{-\bullet}$ are formed within 1 ps, following laser excitation, due to the formation of a CRIP.[21] It is reasonable that the CRIP formation rate constant may slow considerably at 85 K as a result of

losing the dielectric stabilization of the CRIP provided by the solvent, when the solvent is immobilized.[64] This is consistent with the observation that the TREPR spectra are best simulated with $k'_{CS} \cong 10^{11}$ s^{-1}. However, as mentioned above, studies of hole-arrival times at room temperature for stilbene-based D-B-A systems with A-tract bridges[12] show that the arrival time for the hole on G for **SaG7** is more than an order of magnitude faster than charge recombination of the **Aq$^{-\bullet}$G1$^{+\bullet}$** CRIP. Thus the similarity of the k'_{CS} values obtained from simulations of the **Aq$^{-\bullet}$G$n^{+\bullet}$** (n = 2−5) TREPR spectra indicates that $k'_{CS} \cong k_{CS}$, the rate constant for the formation of the initial CRIP at 85 K, i.e., **Aq$^{-\bullet}$A$^{+\bullet}$A$_{n\text{-}2}$Gn** (n = 2−5). Subsequent, charge hopping leading to trapping of the hole on G is sufficiently rapid to maintain the initial ESP of the triplet radical pair.

CONCLUSION

The unusual bimodal distance dependence of charge recombination for the bridge-separated radical ion pairs formed from the **AqGn** capped hairpins (Figure 9) is a consequence of a change in mechanism from rate-determining RP-ISC for $n < 4$ to rate-determining coherent superexchange for $n > 4$. RP-ISC rate constants increase with increasing Aq−G distance, resulting in an inverted distance dependence of k_{CR2} for **AqG2**−**AqG4**. Values of k_{CR2} for **AqG4**−**AqG6** are similar to those for charge recombination in charge-separated stilbene-guanine radical ion pairs generated by charge transfer from singlet stilbene-dicarboxamide to guanine.

The TREPR spectra of **AqGn** are asymmetric with respect to the spin polarization phase pattern of absorption and enhanced emission (A/E) due to the different triplet sublevel populations. The strong dependency of the radical ion pair spectra on the anisotropic nature of triplet-initiated charge separation process allows a complete determination of the initial charge separation rate constant to produce the CRIP (k_{CS}), as well as the dipolar parameters (d, θ, and φ) and the spin−spin exchange coupling (J) in the SRIP. Analysis of the spectra reveal that the triplet-born SRIPs depend strongly on d and weakly on J. The anisotropic properties of the triplet SRIP allow a direct determination of the Aq$^{-\bullet}$ orientation with respect to G$^{+\bullet}$, indicating that Aq$^{-\bullet}$ is not rotating freely but is π-stacked with its neighboring base-pair in the **Aq$^{-\bullet}$G$n^{+\bullet}$** radical ion pairs. Our results show that it is possible to obtain a more complete picture of the structure and dynamics of charge transfer and transport in DNA using complementary transient optical and EPR spectroscopic techniques.

ASSOCIATED CONTENT

Ⓢ Supporting Information
Experimental details including synthesis, absorption spectra, additional transient absorption spectra and kinetics, and computational methods for simulating the spin-polarized EPR spectra. This material is available free of charge via the Internet at http://pubs.acs.org.

AUTHOR INFORMATION

Corresponding Author
m-wasielewski@northwestern.edu; fdl@northwestern.edu; sykobor@ipc.shizuoka.ac.jp
Notes
The authors declare no competing financial interest.

ACKNOWLEDGMENTS

REFERENCES

(1) Lewis, F. D. In *Electron Transfer in Chemistry*; Balzani, V., Ed.; Wiley-VCH: Weinheim, Germany, 2001; Vol. 3, p 105.

(2) *Long-Range Charge Transfer in DNA*; Schuster, G. B., Ed.; Springer-Verlag: Berlin, 2004; Vol. 236−237.

(3) Lewis, F. D.; Letsinger, R. L.; Wasielewski, M. R. *Acc. Chem. Res.* **2001**, *34*, 159.

(4) Lewis, F. D.; Wasielewski, M. R. In *Charge Transfer in DNA*; Wagenknecht, H. A., Ed.; Wiley-VCH: Weinheim, 2005; p 93.

(5) Kawai, K.; Majima, T. *Top. Cur. Chem.* **2004**, *236*, 117.

(6) Genereux, J. C.; Barton, J. K. *Chem. Rev.* **2010**, *110*, 1642.

(7) Vura-Weis, J.; Wasielewski, M. R.; Thazhathveetil, A. K.; Lewis, F. D. *J. Am. Chem. Soc.* **2009**, *131*, 9722.

(8) Conron, S. M. M.; Thazhathveetil, A. K.; Wasielewski, M. R.; Burin, A. L.; Lewis, F. D. *J. Am. Chem. Soc.* **2010**, *132*, 14388.

(9) Blaustein, G. S.; Lewis, F. D.; Burin, A. L. *J. Phys. Chem. B* **2010**, *114*, 6732.

(10) Lewis, F. D.; Kalgutkar, R. S.; Wu, Y.; Liu, X.; Liu, J.; Hayes, R. T.; Wasielewski, M. R. *J. Am. Chem. Soc.* **2000**, *122*, 12346.

(11) Lewis, F. D.; Daublain, P.; Cohen, B.; Vura-Weis, J.; Shafirovich, V.; Wasielewski, M. R. *J. Am. Chem. Soc.* **2007**, *129*, 15130.

(12) Lewis, F. D.; Zhu, H.; Daublain, P.; Cohen, B.; Wasielewski, M. R. *Angew. Chem., Int. Ed.* **2006**, *45*, 7982.

(13) Kawai, K.; Hayashi, M.; Majima, T. *J. Am. Chem. Soc.* **2012**, *134*, 4806.

(14) Takada, T.; Kawai, K.; Cai, X.; Sugimoto, A.; Fujitsuka, M.; Majima, T. *J. Am. Chem. Soc.* **2004**, *126*, 1125.

(15) Lewis, F. D.; Zhu, H.; Daublain, P.; Fiebig, T.; Raytchev, M.; Wang, Q.; Shafirovich, V. *J. Am. Chem. Soc.* **2006**, *128*, 791.

(16) Schuster, G. B. *Acc. Chem. Res.* **2000**, *33*, 253.

(17) Schuster, G. B.; Landman, U. *Top. Cur. Chem.* **2004**, *236*, 139.

(18) Fahlman, R. P.; Sharma, R. D.; Sen, D. *J. Am. Chem. Soc.* **2002**, *124*, 12477.

(19) Bergeron, F.; Nair, V. K.; Wagner, J. R. *J. Am. Chem. Soc.* **2006**, *128*, 14798.

(20) Kawai, K.; Osakada, Y.; Matsutani, E.; Majima, T. *J. Phys. Chem. B* **2010**, *114*, 10195.

(21) Lewis, F. D.; Thazhathveetil, A. K.; Zeidan, T. A.; Vura-Weis, J.; Wasielewski, M. R. *J. Am. Chem. Soc.* **2010**, *132*, 444.

(22) Zeidan, T. A.; Carmieli, R.; Kelley, R. F.; Wilson, T. M.; Lewis, F. D.; Wasielewski, M. R. *J. Am. Chem. Soc.* **2008**, *130*, 13945.

(23) Carmieli, R.; Zeidan, T. A.; Kelley, R. F.; Mi, Q.; Lewis, F. D.; Wasielewski, M. R. *J. Phys. Chem. A* **2009**, *113*, 4691.

(24) Closs, G. L.; Forbes, M. D. E.; Norris, J. R. *J. Phys. Chem.* **1987**, *91*, 3592.

(25) Hore, P. J.; Hunter, D. A.; McKie, C. D.; Hoff, A. J. *Chem. Phys. Lett.* **1987**, *137*, 495.

(26) Buckley, C. D.; Hunter, D. A.; Hore, P. J.; McLauchlan, K. A. *Chem. Phys. Lett.* **1987**, *135*, 307.

(27) Kobori, Y.; Fuki, M.; Murai, H. *J. Phys. Chem. B* **2010**, *114*, 14621.

(28) Lewis, F. D.; Zhu, H.; Daublain, P.; Sigmund, K.; Fiebig, T.; Raytchev, M.; Wang, Q.; Shafirovich, V. *Photochem. Photobiol. Sci.* **2008**, *7*, 534.

(29) Gasper, S. M.; Schuster, G. B. *J. Am. Chem. Soc.* **1997**, *119*, 12762.

(30) Yoshizawa, S.; Kawai, G.; Watanabe, K.; Miura, K.; Hirao, I. *Biochemistry* **1997**, *36*, 4761.

(31) Thazhathveetil, A. K.; Trifonov, A.; Wasielewski, M. R.; Lewis, F. D. *J. Am. Chem. Soc.* **2011**, *133*, 11485.

(32) *MATLAB*; The MathWorks, Inc.: Natick, MA, 2006.

(33) van Ramesdonk, H. J.; Bakker, B. H.; Groeneveld, M. M.; Verhoeven, J. W.; Allen, B. D.; Rostron, J. P.; Harriman, A. *J. Phys. Chem. A* **2006**, *110*, 13145.

(34) Murai, H.; Minami, M.; Hayashi, T.; I'Haya, Y. J. *Chem. Phys.* **1985**, *93*, 333.

(35) Tuma, J.; Paulini, R.; Rojas Stütz, J. A.; Richert, C. *Biochemistry* **2004**, *43*, 15680.

(36) Zhang, L.; Zhu, H.; Sajimon, M. C.; Stutz, J. A. R.; Siegmund, K.; Richert, C.; Shafirovich, V.; Lewis, F. D. *J. Chin. Chem. Soc. (Taipei)* **2006**, *53*, 1501.

(37) Patra, A.; Richert, C. *J. Am. Chem. Soc.* **2009**, *131*, 12671.

(38) Lewis, F. D.; Zhang, L.; Liu, X.; Zuo, X.; Tiede, D. M.; Long, H.; Schatz, G. S. *J. Am. Chem. Soc.* **2005**, *127*, 14445.

(39) Ly, D.; Kan, Y. Z.; Armitage, B.; Schuster, G. B. *J. Am. Chem. Soc.* **1996**, *118*, 8747.

(40) Sanii, L.; Schuster, G. B. *J. Am. Chem. Soc.* **2000**, *122*, 11545.

(41) Lewis, F. D.; Wu, T.; Liu, X.; Letsinger, R. L.; Greenfield, S. R.; Miller, S. E.; Wasielewski, M. R. *J. Am. Chem. Soc.* **2000**, *122*, 2889.

(42) Kobayashi, K.; Tagawa, S. *J. Am. Chem. Soc.* **2003**, *125*, 10213.

(43) McConnell, H. M. *J. Chem. Phys.* **1961**, *35*, 508.

(44) Jortner, J.; Bixon, M.; Langenbacher, T.; Michel-Beyerle, M. E. *Proc. Natl. Acad. Sci. U.S.A.* **1998**, *95*, 12759.

(45) Miura, T.; Wasielewski, M. R. *J. Am. Chem. Soc.* **2011**, *133*, 2844.

(46) Koptyug, I. V.; Lukzen, N. N.; Bagryanskaya, E. G.; Doctorov, A. B. *Chem. Phys. Lett.* **1990**, *175*, 467.

(47) Shushin, A. I. *Chem. Phys. Lett.* **1991**, *181*, 274.

(48) Schluepmann, J.; Lendzian, F.; Plato, M.; Moeblus, K. *J. Chem. Soc., Faraday Trans.* **1993**, *89*, 2853.

(49) Fukuju, T.; Yashiro, H.; Maeda, K.; Murai, H.; Azumi, T. *J. Phys. Chem. A* **1997**, *101*, 7783.

(50) Ito, T.; Naka, M.; Miura, A.; Ujiie, T.; Nakamura, H.; Matsuo, T. *Bull. Chem. Soc. Jpn.* **2001**, *74*, 657.

(51) Marcus, R. A. *J. Chem. Phys.* **1965**, *43*, 679.

(52) Jortner, J. *J. Chem. Phys.* **1976**, *64*, 4860.

(53) Hopfield, J. J. *Proc. Natl. Acad. Sci. U.S.A.* **1974**, *71*, 3640.

(54) Takada, T.; Kawai, K.; Fujitsuka, M.; Majima, T. *Chem.—Eur. J.* **2005**, *11*, 3835.

(55) McGlynn, S. P.; Azumi, T.; Kinoshita, M. *Molecular Spectroscopy of the Triplet State (Prentice-Hall International Series in Chemistry)*; Prentice-Hall: Englewood Cliffs, NJ, 1969.

(56) Kobori, Y.; Shibano, Y.; Endo, T.; Tsuji, H.; Murai, H.; Tamao, K. *J. Am. Chem. Soc.* **2009**, *131*, 1624.

(57) Akiyama, K.; Tero-Kubota, S.; Ikoma, T.; Ikegami, Y. *J. Am. Chem. Soc.* **1994**, *116*, 5324.

(58) Norris, J. R.; Morris, A. L.; Thurnauer, M. C.; Tang, J. *J. Chem. Phys.* **1990**, *92*, 4239.

(59) Efimova, O.; Hore, P. J. *Biophys. J.* **2008**, *94*, 1565.

(60) Kobori, Y.; Fuki, M. *J. Am. Chem. Soc.* **2011**, *133*, 16770.

(61) Adhikary, A.; Kumar, A.; Becker, D.; Sevilla, M. D. *J. Phys. Chem. B* **2006**, *110*, 24171.

(62) Salikhov, K. M.; Zech, S. G.; Stehlik, D. *Mol. Phys.* **2002**, *100*, 1311.

(63) Kobori, Y.; Sekiguchi, S.; Akiyama, K.; Tero-Kubota, S. *J. Phys. Chem. A* **1999**, *103*, 5416.

(64) Gaines, G. L., III; O'Neil, M. P.; Svec, W. A.; Niemczyk, M. P.; Wasielewski, M. R. *J. Am. Chem. Soc.* **1991**, *113*, 719.